International Journal of Solids and Structures 51 (2014) 4419–4426

Contents lists available at ScienceDirect

International Journal of Solids and Structures

journal homepage: www.elsevier.com/locate/ijsolstr

# Energy release rates in rubber during dynamic crack propagation

Martin Kroon *

*Department of Solid Mechanics, Royal Institute of Technology, Osquars backe 1, SE-100 44 Stockholm, Sweden*

ARTICLE INFO

*Article history:*
Received 24 July 2013
Received in revised form 26 April 2014
Available online 28 September 2014

*Keywords:*
Rubber
Elastomer
Fracture mechanics
Steady
Crack
Viscoelasticity

ABSTRACT

The theoretical understanding of the fracture mechanics of rubber is not as well developed as for other engineering materials, such as metals. The present study is intended to further the understanding of the dissipative processes that take place in rubber in the vicinity of a propagating crack tip. This dissipation contributes significantly to the total fracture toughness of the rubber and is therefore of great interest from a fracture mechanics point of view. To study this, a computational framework for analysing high-speed crack growth in a biaxially stretched rubber under plane stress is therefore formulated. The main purpose is to investigate the energy release rates required for crack propagation under different modes of biaxial stretching. The results show, that inertia comes into play when the crack speed exceeds about 50 m/s. The total work of fracture by far exceeds the surface energy consumed at the very crack tip, and the difference must be attributed to dissipative damage processes in the vicinity of the crack tip. The size of this damage/dissipation zone is expected to be a few millimetres.

© 2014 Elsevier Ltd. All rights reserved.

## 1. Introduction

Fracture mechanics of metals has been studied extensively both experimentally and theoretically over the years. When it comes to rubber, several experimental investigations have been made, e.g. Rivlin and Thomas (1953), Thomas (1955), Greensmith and Thomas (1955), Greensmith (1956), Kolsky (1969), Gent and Kim (1978), Gent and Marteny (1982a), Dragoni and Medri (1988), Chung et al. (1991), Deegan et al. (2002), Petersan et al. (2004), Zhang et al. (2009), Niemczura and Ravi-Chandar (2011) and Chen et al. (2011). Several of the early studies aimed at establishing a critical tearing energy for rubber. Other studies have tried to determine the crack speed as a function of the applied (macroscopic) load state. Additional information has been provided in other studies that have performed microscopic investigations of the fracture surfaces of rubber (Bascom, 1977; Fukahori and Andrews, 1978; Bhowmick et al., 1980; Setua and De, 1983; Gent and Pulford, 1984; Goldberg et al., 1988; Pandey and Mathur, 2003). However, the theoretical understanding of fracture in rubber is less developed.

Rubbers may be characterised as viscoelastic, which means that viscoelastic dissipation contributes to the total fracture toughness of the material. Hence, there are at least two different sources for energy consumption at an advancing crack tip in rubber. The first source is associated with the innermost region at the crack tip, where cavities form, polymer chains are pulled out, and polymer chain bonds are broken. This process is mainly governed by the basic molecular structure and strength of the material (Thomas, 1994). The second source is the viscoelastic dissipation in the polymer in front of the crack tip (Persson et al., 2005). Possibly some amount of damage may also be involved. On the basis of these observations, it is to be expected that the tearing energy of rubber will depend strongly on both temperature and crack velocity.

It has also been noted that transverse stretching (i.e. stretching in the direction of crack extension and propagation) tends to decrease the energy release rate for propagating cracks (Gent and Kim, 1978; Gent and Marteny, 1982a). In fact, rubber sheets that are highly stretched in the transverse direction can be split apart quite easily. This indicates that the originally isotropic material becomes fibrous in character, i.e. much weaker for a tear running in the direction of extension than for one running at right angles to it.

There are a few theoretical studies that examine the contribution of viscoelasticity to the fracture toughness of polymers, e.g. Carbone and Persson (2005), Marder (2005, 2006), Persson and Brener (2005), Wang and Chen (2005), Tang et al. (2008, 2009), Kroon (2011), Elmukashfi and Kroon (2012) and Elmukashfi and Kroon (in press). However, several of these studies adopt a theory valid for infinitesimal strains, and the validity of those results for rubber-like solids is therefore questionable. In a previous study by the present author (Kroon, 2011), dynamic crack propagation under steady-state conditions in rubber was examined. Plane deformation was assumed and a Kelvin-type of material was

* Tel.: +46 8 7907553; fax: +46 8 4112418.
*E-mail address:* martin@hallf.kth.se

http://dx.doi.org/10.1016/j.ijsolstr.2014.09.010
0020-7683/© 2014 Elsevier Ltd. All rights reserved.

adopted. It was demonstrated that viscoelastic dissipation may explain the large discrepancies observed between the surface energy consumed at the very crack tip and the macroscopic fracture toughness obtained in experiments. Other theoretical studies address different aspects of crack growth in viscoelastic solids, mostly under the assumption of infinitesimal strains (Knauss, 1969; Lindley, 1973; Schapery, 1975, 1989; de Gennes, 1996; Rahulkumar et al., 2000).

In the present work, a computational framework is proposed for analysing high-speed crack propagation in biaxially stretched rubber sheets under conditions of steady-state and plane stress. The main purpose of the study is to shed some more light on the contributions from local surface energy at the crack tip and bulk viscoelasticity and possible damage processes to the total work of fracture required to propagate a crack. The problem to be analysed is formulated in Section 2 and the numerical implementation is outlined in Section 3. Numerical results are presented in Section 4 and discussed in Section 5.

## 2. Problem formulation

### 2.1. Geometry and boundary conditions

Consider a crack that propagates through a rubber solid at a constant speed and under steady-state conditions. The crack is illustrated in Fig. 1(a). At some point the crack passes through the control volume, indicated by the dotted box in Fig. 1(a). This rectangular control volume is analysed, and its dimensions and the applied boundary conditions are indicated in Fig. 1(b). Due to symmetry, only the upper half of the control volume is modelled. The coordinate system $X_1$–$X_2$–$X_3$ pertains to the reference configuration and is located at the propagating crack tip. Position vectors $\mathbf{x} = x_i\mathbf{e}_i$ and $\mathbf{X} = X_i\mathbf{e}_i$ are associated with the deformed and reference configurations, respectively, where $\mathbf{e}_i$ is a set of orthogonal basis vectors. The displacement vector is defined as $\mathbf{u} = \mathbf{x} - \mathbf{X}$, and the traction vector $\mathbf{T}$ is defined as force per unit undeformed area. Boundary conditions are applied according to

$$X_1 = \pm B_0 \ : u_1 = \pm\Delta_1, \quad T_2 = 0, \tag{1}$$
$$X_1 > 0, \quad X_2 = 0 \ : u_2 = 0, \quad T_1 = 0, \tag{2}$$
$$X_1 < 0, \quad X_2 = 0 \ : T_1 = T_2 = 0, \tag{3}$$
$$X_2 = H_0 \ : u_2 = \Delta_2, \quad T_1 = 0, \tag{4}$$

i.e. loading is imposed in terms of the prescribed displacements $\Delta_1$ and $\Delta_2$. In addition, plane stress is assumed, implying that $T_3 = 0 \ \forall \ \mathbf{X}$.

The applied boundary displacements correspond to the global stretches

$$\Lambda_1 = \frac{B_0 + \Delta_1}{B_0}, \quad \Lambda_2 = \frac{H_0 + \Delta_2}{H_0}. \tag{5}$$

### 2.2. Equations of motion

We assume that steady-state prevails, and the fundamental assumption is made that the time derivative of all field variables can be computed as

$$\frac{\mathrm{d}(\bullet)}{\mathrm{d}t} = -V_c\frac{\partial(\bullet)}{\partial X_1}, \tag{6}$$

where $V_c$ is the Lagrangian speed of the crack in the reference configuration. The true crack speed $v_c$ relates to the Lagrangian speed as

$$v_c = V_c\Lambda_1. \tag{7}$$

The equations of motion may be expressed as

$$\frac{\partial P_{ij}}{\partial X_j} = \rho_0\frac{\mathrm{d}^2u_i}{\mathrm{d}t^2} = \rho_0 V_c^2\frac{\partial^2 u_i}{\partial X_1^2}, \tag{8}$$

where $P_{ij}$ are the components of the first Piola–Kirchhoff stress tensor, and $\rho_0$ is the density of the material in the undeformed state. Body forces are ignored. Multiplication with a virtual displacement field $\delta u_i$ and integration over the control volume domain $\Omega_0$ gives

$$\int_{\Omega_0}\left(\frac{\partial P_{ij}}{\partial X_j} - \rho_0 V_c^2\frac{\partial^2 u_i}{\partial X_1^2}\right)\delta u_i \mathrm{d}\Omega_0 = 0. \tag{9}$$

By use of the chain rule and Gauss' theorem, Eq. (9) may be recast into

$$\int_{\Omega_0}\left(P_{ij} - \rho_0 V_c^2\frac{\partial u_i}{\partial X_1}\delta_{1j}\right)\frac{\partial\delta u_i}{\partial X_j}\mathrm{d}\Omega_0 + \int_{S_0}\left(\rho_0 V_c^2\frac{\partial u_i}{\partial X_1}N_1 - T_i\right)\delta u_i \mathrm{d}S_0 = 0, \tag{10}$$

where $\delta_{ij}$ is the Kronecker delta, $S_0$ is the boundary surface of the control volume in the reference configuration, $N_i$ is the outward normal to $S_0$, and $T_i = P_{ij}N_j$ is the traction vector acting on $S_0$. We also note that

$$P_{ij}\frac{\partial\delta u_i}{\partial X_j} = P_{ij}\delta F_{ij} = S_{ij}\delta E_{ij}, \tag{11}$$

where $F_{ij} = \partial x_i/\partial X_j$, $S_{ij}$, and $E_{ij}$ are the components of the deformation gradient tensor, the second Piola–Kirchhoff stress tensor, and the Green strain tensor, respectively. Application of the boundary

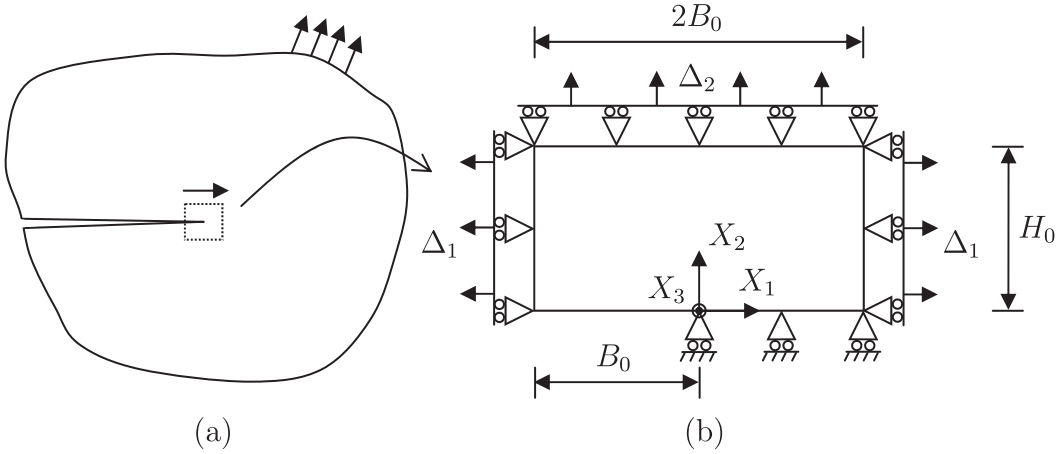



**Fig. 1.** (a) Crack propagating through a rubber solid. (b) Geometry and boundary conditions of the analysed control volume.

conditions Eqs. (1)–(4) means that the last integral over $S_0$ in Eq. (10) vanishes, since $\delta u_i$ is zero where prescribed displacements are applied and $N_1$ and $T_i$ vanish on the free crack surface. Eq. (10) may now be rewritten and simplified to

$$\mathcal{F}(\mathbf{u},\delta\mathbf{u}) = \int_{\Omega_0}\left(S_{ij}\delta E_{ij} - \rho_0 V_c^2 \frac{\partial u_i}{\partial X_1}\frac{\partial \delta u_i}{\partial X_1}\right)\mathrm{d}\Omega_0 = 0, \tag{12}$$

which constitutes the weak form of the equations of motion for the present steady-state problem.

### 2.3. Constitutive behaviour

The total deformation gradient $\mathbf{F}$ is split into a viscous and an elastic part, $\mathbf{F}_v$ and $\mathbf{F}_e$, such that

$$\mathbf{F} = \mathbf{F}_e\mathbf{F}_v \tag{13}$$

and incompressibility is assumed, implying that $\det\mathbf{F} = \det\mathbf{F}_e = \det\mathbf{F}_v \equiv 1$. The associated right Cauchy–Green deformation tensors are defined as $\mathbf{C} = \mathbf{F}^T\mathbf{F}$, $\mathbf{C}_v = \mathbf{F}_v^T\mathbf{F}_v$, and $\mathbf{C}_e = \mathbf{F}_e^T\mathbf{F}_e$. Plane stress is taken to prevail, and the components of the deformation gradient $\mathbf{F}$, the right Cauchy–Green deformation tensor $\mathbf{C}$, and the internal state variable tensor $\mathbf{C}_v$ are assumed to be on the forms

$$F_{ij} = \begin{bmatrix} F_{11} & F_{12} & 0 \\ F_{21} & F_{22} & 0 \\ 0 & 0 & F_{33}\end{bmatrix}, \quad C_{ij} = \begin{bmatrix} C_{11} & C_{12} & 0 \\ C_{21} & C_{22} & 0 \\ 0 & 0 & C_{33}\end{bmatrix}, \quad C_{v,ij} = \begin{bmatrix} C_{v,11} & C_{v,12} & 0 \\ C_{v,21} & C_{v,22} & 0 \\ 0 & 0 & C_{v,33}\end{bmatrix}. \tag{14}$$

The constitutive behaviour of the material is formulated in terms of a strain energy function $\Psi$:

$$\Psi = \frac{\mu_e}{2(\alpha+1)}\left(I_1^{\alpha+1} - 3^{\alpha+1}\right) + \frac{\mu_v}{2(\alpha+1)}\left(I_v^{\alpha+1} - 3^{\alpha+1}\right) - p(J-1), \tag{15}$$

where $\mu_e$, $\mu_v$, and $\alpha$ are material constants, $J = \det\mathbf{F}$, $p$ is a Lagrange multiplier, and the invariants $I_1$ and $I_v$ are defined as

$$I_1 = \mathbf{C}:\mathbf{I}, \quad I_v = \mathbf{C}_e:\mathbf{I} = \mathbf{C}:\mathbf{C}_v^{-1}, \tag{16}$$

where $\mathbf{I}$ is the identity tensor.

The second Piola–Kirchhoff stress is computed as $\mathbf{S} = 2\partial\Psi/\partial\mathbf{C}$, and after the Lagrange multiplier has been determined by use of the boundary condition $S_{33} = 0$, the second Piola–Kirchhoff stress tensor takes on the form

$$\mathbf{S} = \mu_e I_1^{\alpha}\left(\mathbf{I} - C_{33}\mathbf{C}^{-1}\right) + \mu_v I_v^{\alpha}\left(\mathbf{C}_v^{-1} - \frac{C_{33}}{C_{v,33}}\mathbf{C}^{-1}\right). \tag{17}$$

It should be noted that the first term in Eq. (17) (purely elastic stresses) vanishes for $\mathbf{C}\to\mathbf{I}$, whereas the second term (viscoelastic stresses) vanishes for $\mathbf{C}_v\to\mathbf{C}$.

In the present problem, it is assumed that the virgin (unbroken) material is first exposed to a state of biaxial loading, characterised by the global stretches $\Lambda_1$ and $\Lambda_2$, corresponding to the homogeneous deformation state

$$\mathbf{C}_0 = \Lambda_1^2\mathbf{e}_1\otimes\mathbf{e}_1 + \Lambda_2^2\mathbf{e}_2\otimes\mathbf{e}_2 + \frac{1}{\Lambda_1^2\Lambda_2^2}\mathbf{e}_3\otimes\mathbf{e}_3. \tag{18}$$

When the viscoelastic stresses have been relaxed, the state variable tensor $\mathbf{C}_v$ will therefore be $\mathbf{C}_v = \mathbf{C}_0$. The viscoelastic relaxation in the rubber material is modelled by use of the tensor $\mathbf{C}_v$, and in principle, an evolution law is required for $\mathbf{C}_v$. However, the time constants associated with stress relaxation in rubber are of the order of a second or higher (Kawabata and Kawai, 1977; Bergström and Boyce, 1998), whereas the processes associated with the dynamic crack propagation to be considered here take place at much shorter time scales (on the order of microseconds). In the present analysis, we therefore neglect the evolution of $\mathbf{C}_v$ and assume that $\mathbf{C}_v = \mathbf{C}_0$ holds throughout the analysis. The second Piola–Kirchhoff stresses may then be expressed as

$$\mathbf{S} = \mu_e I_1^{\alpha}\left(\mathbf{I} - C_{33}\mathbf{C}^{-1}\right) + \mu_v I_v^{\alpha}\left(\mathbf{C}_0^{-1} - C_{33}\Lambda_1^2\Lambda_2^2\mathbf{C}^{-1}\right). \tag{19}$$

From this, the first Piola–Kirchhoff stress tensor $\mathbf{P}$ and Cauchy stress tensor $\boldsymbol{\sigma}$ are computed as

$$\mathbf{P} = \mathbf{FS}, \quad \boldsymbol{\sigma} = \mathbf{PF}^T. \tag{20}$$

The material stiffness tensor is also introduced, whose components are defined as

$$\mathbb{C}_{ijkl} = 2\frac{\partial S_{ij}}{\partial C_{kl}}. \tag{21}$$

### 2.4. J-integral evaluation

The $J$-integral (Rice, 1968; Chang, 1972) is an appropriate entity for quantifying the energy required for crack propagation. The $J$-integral is computed as a line integral around the crack tip as indicated in Fig. 2. In the present problem, where we have both strain energy and kinetic energy involved, the $J$-integral may be expressed as

$$J_{\mathrm{tip}} = \lim_{\Gamma\to 0}\int_{\Gamma}\left(EN_1 - P_{ij}\frac{\partial u_i}{\partial X_1}N_j\right)\mathrm{d}\Gamma, \tag{22}$$

where $E = \Psi + T$ is the internal energy per unit reference volume, $\Psi$ is the strain energy, and $T$ is the kinetic energy. The normal to the curve $\Gamma$ is denoted $N_j$. The notation $J_{\mathrm{tip}}$ indicates that the $J$-integral is evaluated close to the crack tip. The kinetic energy is computed as

$$T = \frac{\rho_0}{2}\dot{u}_i\dot{u}_i = \frac{\rho_0 V_c^2}{2}\frac{\partial u_i}{\partial X_1}\frac{\partial u_i}{\partial X_1}. \tag{23}$$

In the present steady-state problem, the $J$-integral is path-independent, and $J_{\mathrm{tip}}$ may therefore be evaluated by use of a contour $\Gamma_1$ located at some distance from the crack tip, see Fig. 2. The $J$-integral is then computed as

$$J_{\mathrm{tip}} = \int_{\Gamma_1}\left(EN_1' - P_{ij}\frac{\partial u_i}{\partial X_1}N_j'\right)\mathrm{d}\Gamma_1. \tag{24}$$

A derivation of this expression and a proof of the path independence are provided in Kroon (2011).

We will also consider the energy entity $J_{\mathrm{ff}}$, defined as

$$\begin{aligned} J_{\mathrm{ff}} &= \int_{\Gamma_1}\left(\Psi N_1' - P_{ij}\frac{\partial u_i}{\partial X_1}N_j'\right)\mathrm{d}\Gamma_1 \\ &= \int_{X_2=-H_0}^{H_0}\left[\Psi(X_1 = B_0, X_2') - \Psi(X_1 = -B_0, X_2')\right]\mathrm{d}X_2', \end{aligned} \tag{25}$$

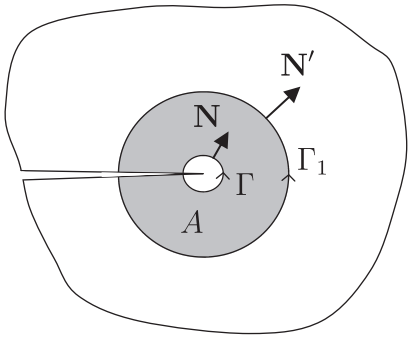



**Fig. 2.** Definitions for evaluation of $J$-integral.

where $X_2'$ is an integration variable and the line contour $\Gamma_1$ is taken to coincide with the edges of the control volume in Fig. 1(b). The resulting value $J_{\mathrm{ff}}$ is often referred to as the 'far field' value of the $J$-integral, and this value corresponds to the energy release rate measured in experiments.

## 3. Numerical implementation

The geometry of the control volume in Fig. 1(b) is discretised and the finite element mesh is shown in Fig. 3. We apply $B_0 = 2H_0$ and the innermost elements at the crack tip are collapsed and have a characteristic size of $l_{\mathrm{e}}$. The model is subdivided into $n_{\mathrm{e}} = n_{\mathrm{r}} n_{\mathrm{a}}$ elements with domains $\Omega_e$, where the subscript $(\bullet)_e$ is an index ($1 \leqslant e \leqslant n_{\mathrm{e}}$) referring to a specific finite element, and $n_{\mathrm{r}}$ and $n_{\mathrm{a}}$ denote the number of elements in the radial and angular directions of the mesh, respectively. Isoparametric elements are employed, and the initial geometry and displacement fields of the model are interpolated according to

$$\underline{\mathbf{X}} = \sum_{I=1}^{n_{\mathrm{node}}} N_I \underline{\mathbf{X}}_I, \quad \underline{\mathbf{u}} = \sum_{I=1}^{n_{\mathrm{node}}} N_I \underline{\mathbf{u}}_I, \quad \delta\underline{\mathbf{u}} = \sum_{I=1}^{n_{\mathrm{node}}} N_I \delta\underline{\mathbf{u}}_I, \tag{26}$$

where $\underline{\mathbf{X}}$, $\underline{\mathbf{u}}$, and $\delta\underline{\mathbf{u}}$ denote interpolated position vector, displacement field, and virtual displacement field, respectively, where

$$\underline{\mathbf{X}} = [X_1 \quad X_2]^{\mathrm{T}}, \qquad \underline{\mathbf{u}} = [u_1 \quad u_2]^{\mathrm{T}}, \qquad \delta\underline{\mathbf{u}} = [\delta u_1 \quad \delta u_2]^{\mathrm{T}}. \tag{27}$$

Indexation $(\bullet)_I$ denotes nodal values of the respective entities, and linear shape functions $N_I$ are employed ($n_{\mathrm{node}} = 4$). In the following, underlined entities denote the finite element representation of an entity. The position vector in the current configuration is computed as $\underline{\mathbf{x}} = \underline{\mathbf{X}} + \underline{\mathbf{u}}$.

The variation of the Green strain is represented as

$$\delta\underline{\mathbf{E}} = \sum_{I=1}^{n_{\mathrm{node}}} \underline{\mathbf{B}}_I \delta\underline{\mathbf{u}}_I, \quad \underline{\mathbf{B}}_I = \begin{bmatrix} N_{I,1}\underline{\mathbf{x}}_{,1}^{\mathrm{T}} \\ N_{I,2}\underline{\mathbf{x}}_{,2}^{\mathrm{T}} \\ N_{I,1}\underline{\mathbf{x}}_{,2}^{\mathrm{T}} + N_{I,2}\underline{\mathbf{x}}_{,1}^{\mathrm{T}} \end{bmatrix}, \tag{28}$$

where $\underline{\mathbf{E}} = [E_{11} \quad E_{22} \quad 2E_{12}]^{\mathrm{T}}$ represents the (2D) Green–Lagrange strain tensor $\mathbf{E}$, and $\underline{\mathbf{B}}_I$ is the standard gradient operator associated with the $I$th node. Above we have also introduced the notation $(\bullet)_{,i} = \partial(\bullet)/\partial X_i$.

On the basis of Eq. (12), the equations of motion for an element may now be expressed as

$$\sum_{I=1}^{n_{\mathrm{node}}} \delta\underline{\mathbf{u}}_I^{\mathrm{T}} \int_{\Omega_{\mathrm{e}}} \left( \underline{\mathbf{B}}_I^{\mathrm{T}} \underline{\mathbf{S}} - \rho_0 V_{\mathrm{c}}^2 N_{I,1} \underline{\mathbf{u}}_{,1} \right) \mathrm{d}\Omega_{\mathrm{e}} = 0, \tag{29}$$

where $\underline{\mathbf{S}} = [S_{11} \quad S_{22} \quad S_{12}]^{\mathrm{T}}$ is the finite element representation of the second Piola–Kirchhoff stress tensor. The stiffness matrix for an element is denoted $\underline{\mathbf{K}}_{IJ}$, where $I, J = 1, \ldots, n_{\mathrm{node}}$, and it takes on the form

$$\underline{\mathbf{K}}_{IJ} = \int_{\Omega_{\mathrm{e}}} \left\{ \underline{\mathbf{B}}_I^{\mathrm{T}} \underline{\mathbb{C}} \underline{\mathbf{B}}_J + \left( N_{I,i} S_{ij} N_{J,j} - \rho_0 V_{\mathrm{c}}^2 N_{I,1} N_{J,1} \right) \mathbf{I} \right\} \mathrm{d}\Omega_{\mathrm{e}}, \tag{30}$$

where $\mathbf{I}$ is the unit matrix. The material stiffness matrix $\underline{\mathbb{C}}$ takes on the form

$$\underline{\mathbb{C}} = \begin{bmatrix} \frac{\partial S_{11}}{\partial E_{11}} & \frac{\partial S_{11}}{\partial E_{22}} & \frac{\partial S_{11}}{\partial (2E_{12})} \\ \frac{\partial S_{22}}{\partial E_{11}} & \frac{\partial S_{22}}{\partial E_{22}} & \frac{\partial S_{22}}{\partial (2E_{12})} \\ \frac{\partial S_{12}}{\partial E_{11}} & \frac{\partial S_{12}}{\partial E_{22}} & \frac{\partial S_{12}}{\partial (2E_{12})} \end{bmatrix}. \tag{31}$$

The area element in the integration is computed as $\mathrm{d}\Omega_{\mathrm{e}} = |\mathbf{G}_\xi \times \mathbf{G}_\eta| \, \mathrm{d}\xi \mathrm{d}\eta$, where $\mathbf{G}_\xi = \partial\underline{\mathbf{X}}/\partial\xi$, $\mathbf{G}_\eta = \partial\underline{\mathbf{X}}/\partial\eta$, and $\xi$ and $\eta$ are the natural coordinates of the isoparametric element. Derivatives with respect to the Cartesian coordinates $X_i$ are computed as

$$\underline{\mathbf{u}}_{,i} = \sum_{I=1}^{n_{\mathrm{node}}} N_{I,i} \underline{\mathbf{u}}_I, \quad \underline{\mathbf{x}}_{,i} = \sum_{I=1}^{n_{\mathrm{node}}} N_{I,i} \underline{\mathbf{x}}_I, \tag{32}$$

where the derivatives of the shape functions are computed as

$$\begin{bmatrix} N_{I,1} \\ N_{I,2} \end{bmatrix} = \begin{bmatrix} \mathbf{G}_\xi^{\mathrm{T}} \\ \mathbf{G}_\eta^{\mathrm{T}} \end{bmatrix}^{-1} \begin{bmatrix} N_{I,\xi} \\ N_{I,\eta} \end{bmatrix}. \tag{33}$$

Standard Gauss integration (four integration points) is used to evaluate Eqs. (29) and (30), and contributions from all elements are assembled in standard ways. The global system of equations is then solved by use of a Newton–Raphson scheme.

When evaluating the $J$-integral, we adopt the domain integration method (Li et al., 1985; Shih et al., 1986; Chang and Chen, 1997; Rajaram et al., 2000). A smooth function $q_1$ is introduced, and $J$ is computed as

$$J = \int_A \left( P_{ij} \frac{\partial u_i}{\partial X_1} - E\delta_{1j} \right) \frac{\partial q_1}{\partial X_j} \mathrm{d}A, \tag{34}$$

where $A$ is the area enclosed by the contours $\Gamma$, $\Gamma_1$, and the two load-free crack faces, see Fig. 2. An explanation of Eq. (34) is provided in Kroon (2011). A similar expression is used for evaluating $J_{\mathrm{ff}}$. The weight function $q_1$ must be 1 along $\Gamma$ and 0 along $\Gamma_1$. Half rings of elements, starting from the symmetry plane ($X_2 = 0$) and ending at the free crack surface, were defined, and the area $A$ was comprised of consecutive element half-rings. The weight function $q_1$ was chosen to be 1 over all element rings included in $A$, except for the outermost ring, where $q_1$ decreased linearly to zero. Hence, only the outermost element ring had to be considered when evaluating Eq. (34). Integration of Eq. (34) was done by use of the same standard Gauss integration that was used for the global FE system.

## 4. Numerical results

### 4.1. Determination of parameters in constitutive law

Experimental results are taken from Gent and Kim (1978) and Gent and Marteny (1982a,b), in which tests are performed on a filled natural rubber. Test pieces were tested in uniaxial tension, see Fig. 4. In a uniaxial test, the deformation gradient is $\mathbf{F} = \lambda_1^0 \mathbf{e}_1 \otimes \mathbf{e}_1 + 1/\sqrt{\lambda_1^0}\mathbf{e}_2 \otimes \mathbf{e}_2 + 1/\sqrt{\lambda_1^0}\mathbf{e}_3 \otimes \mathbf{e}_3$, where $\lambda_1$ is the stretch imposed in the loading direction. Furthermore, in a long-term response uniaxial tensile test, the first Piola–Kirchhoff stress is predicted to be

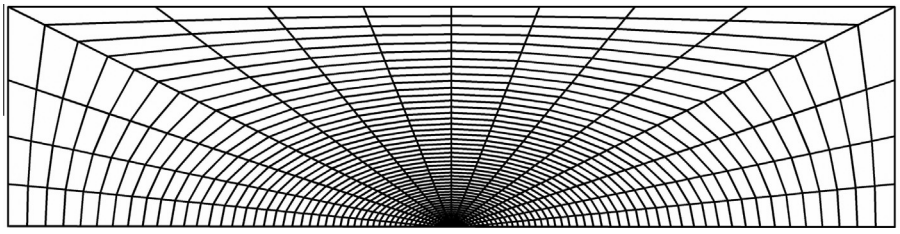


**Fig. 3.** Finite element mesh.

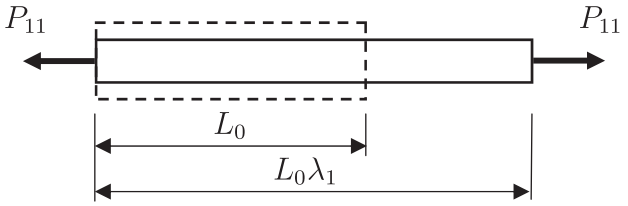



**Fig. 4.** Uniaxial stretching.

$$P_{11} = \mu_e I_1^{\alpha}\left(\lambda_1 - \frac{1}{\lambda_1^2}\right). \tag{35}$$

Fig. 5 shows the experimental outcome from a long-term response uniaxial tensile test (Gent and Kim, 1978) together with the fitted constitutive model. This yielded the parameter estimates $\mu_e = 1.1$ MPa and $\alpha = 0.5$.

In addition, retraction velocity tests were made on the same material (Gent and Marteny, 1982b). In these tests, a stretch $\lambda_1^0$ was first applied. The test strip was then released in one end, which allowed the stresses in the specimen to contract the strip dynamically. After one end had been released, there was a short initial acceleration of the free end, but the retraction speed $v_r$ soon reached a fairly constant level. In these tests, the retraction speed is defined as

$$v_r = -L_0\dot{\lambda}_1, \tag{36}$$

where $L_0 = 0.25$ m. In the expressions for the stresses in the material, we assume that $\mathbf{C}_v = \mathbf{C}_0 = (\lambda_1^0)^2\mathbf{e}_1 \otimes \mathbf{e}_1 + 1/\lambda_1^0\mathbf{e}_2 \otimes \mathbf{e}_2 + 1/\lambda_1^0\mathbf{e}_3 \otimes \mathbf{e}_3$.

A short finite element program was written in Matlab to analyse the retraction problem and to predict the retraction speed based on the present constitutive model. In Fig. 6, the predicted retraction speed after the initial acceleration is shown for a few different values of $\mu_v$ together with the experimental data from Gent and Marteny (1982b). Based on these observations, we adopt a value of $\mu_v = 5$ MPa, which gives a relatively good prediction of the retraction speed in the stretch regime of interest.

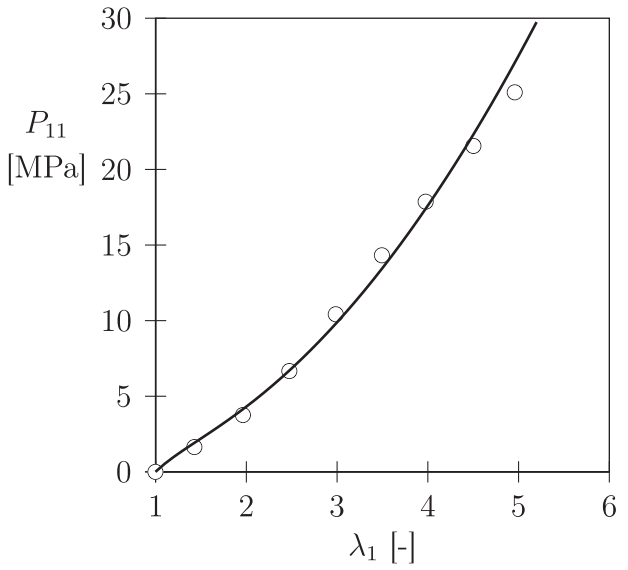



**Fig. 5.** Long-term response in uniaxial tensile test: experimental results (symbols) and fitted model (solid line). Material parameters: $\mu_e = 1.1$ MPa, $\alpha = 0.5$.

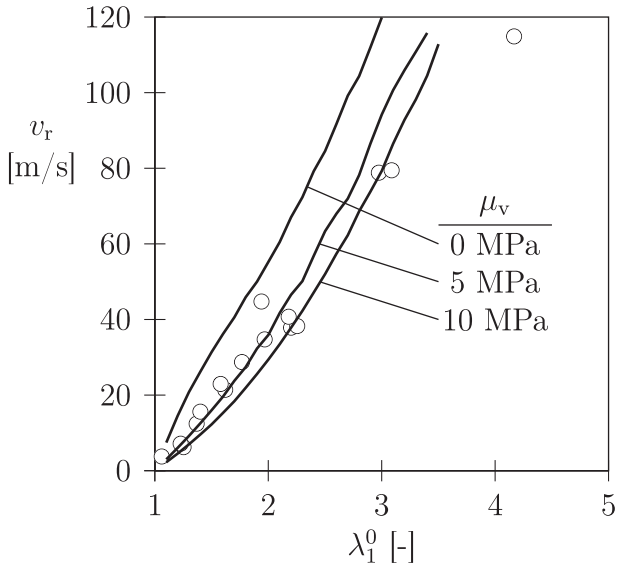



**Fig. 6.** Experimental retraction velocities from Gent and Marteny (1982b) together with model predictions.

### 4.2. Geometric parameters in numerical model

Gent and Marteny (1982a) present experimental results for dynamic crack propagation in biaxially stretched rubber sheets of the material for which the constitutive response was determined in the previous subsection. Rubber sheets are stretched biaxially, such that the applied stretches are $\Lambda_1$ and $\Lambda_2$ in the $X_1$- and $X_2$-directions, respectively, see Fig. 7. A grid was painted on one side of the sheets to measure the applied in-plane strains. The third direction $X_3$ is oriented in the thickness direction of the sheets. The rubber sheets were relatively thin (0.5 mm) compared with the two in-plane dimensions (about 150 mm × 20 mm), and it is

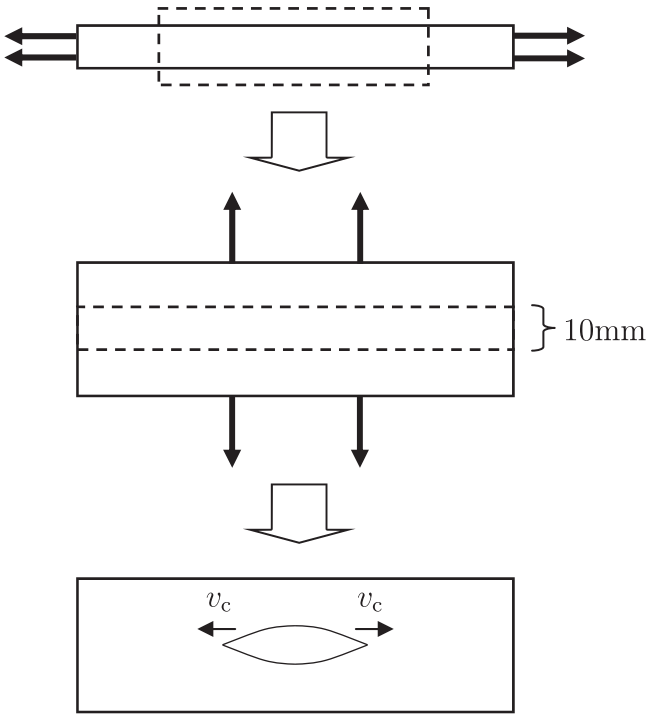



**Fig. 7.** Principle sketch of experimental setup used in Gent and Marteny (1982a).

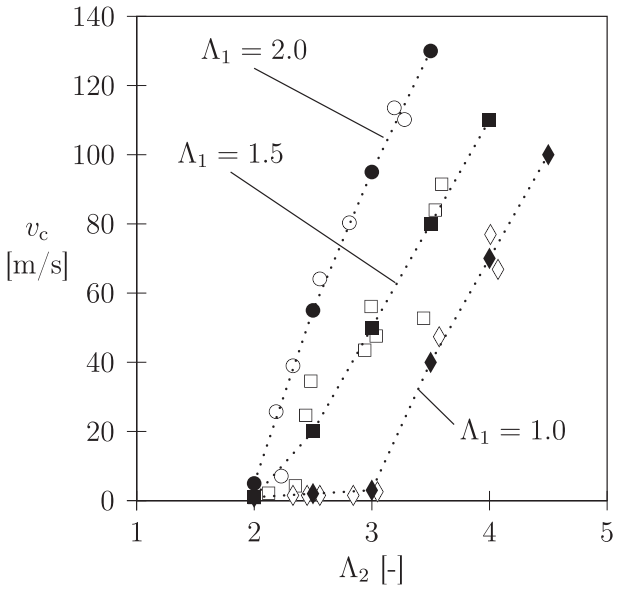



**Fig. 8.** Crack speed vs. applied stretch. Open symbols denote experimental results from Gent and Marteny (1982a), and filled symbols connected with dotted lines denote computational points.

**Table 1**
Energy release rates for computational points in Fig. 8.

| $\Lambda_1$ [–] | $\Lambda_2$ [–] | $v_c$ [m/s] | $J$ [kJ/m$^2$] | $J_{ff}$ [kJ/m$^2$] |
|---|---|---|---|---|
| 1.0 | 2.0 | 1 | 7.84 | 7.84 |
| 1.0 | 2.5 | 2 | 22.3 | 22.3 |
| 1.0 | 3.0 | 3 | 48.6 | 48.6 |
| 1.0 | 3.5 | 40 | 90.1 | 90.2 |
| 1.0 | 4.0 | 70 | 149 | 152 |
| 1.0 | 4.5 | 100 | 228 | 233 |
| 1.5 | 2.0 | 1 | 12.1 | 12.1 |
| 1.5 | 2.5 | 20 | 31.4 | 31.7 |
| 1.5 | 3.0 | 50 | 65.3 | 68.1 |
| 1.5 | 3.5 | 80 | 117 | 128 |
| 1.5 | 4.0 | 110 | 190 | 218 |
| 2.0 | 2.0 | 5 | 17.6 | 17.7 |
| 2.0 | 2.5 | 55 | 42.7 | 46.9 |
| 2.0 | 3.0 | 95 | 84.8 | 104 |
| 2.0 | 3.5 | 130 | 147 | 202 |

justified to assume that a state of plane stress prevails. The biaxial stretch state is imposed as indicated in Fig. 7. Hence, a stretch $\Lambda_1$ is first applied in the $X_1$-direction. After this, the sheet is clamped between two rigid grips separated 10 mm from each other in the $X_2$-direction, and then the stretch $\Lambda_2$ is applied in the $X_2$-direction. After the initial biaxial stretch state has been imposed, a crack is initiated at the centre of the stretched sheet by use of a needle, and the crack starts to grow dynamically in the $X_1$-direction. The crack exhibits a short acceleration phase, but soon it reaches a steady-state and propagates with a constant speed $v_c$. The dimensions of the FE model are chosen to reflect the conditions in the experiments. Hence, the material is assumed to be incompressible, and the height of the model is therefore set to $H_0 = \sqrt{\Lambda_1} \cdot 5$ mm. The smallest elements at the crack tip have a size of $l_e = 0.1$ mm. The results in Gent and Marteny (1982a) are provided in terms of the steady-state crack speed as a function of the applied stretches $\Lambda_1$ and $\Lambda_2$.

### 4.3. Results

The attained crack speeds $v_c$ at different global stretches $\Lambda_1$ and $\Lambda_2$ from Gent and Marteny (1982a) are shown in Fig. 8 (open symbols). There are two major tendencies to be noted in the results in Fig. 8. First of all, the crack speed increases with $\Lambda_2$, i.e. the stretch applied normal to the direction of crack propagation. Secondly, for a given stretch $\Lambda_2$, the crack speed increases with increasing transverse stretch $\Lambda_1$.

Enclosed in Fig. 8 are also a number of states $\{\Lambda_1, \Lambda_2, v_c\}$ (filled symbols connected with dotted lines) that are analysed by use of the computational framework presented in previous sections. The computational points are chosen to be representative of the experimental results. In a few cases, the computational points are obtained through extrapolation rather than interpolation of the experimental values. The results from the analyses are listed in Table 1 in terms of the attained values of $J$ and $J_{ff}$.

The outcomes from two analyses are illustrated in Fig. 9. In this case, the distribution of the main principal (Cauchy) stress is shown. The crack tip profile has the typical parabolic shape often observed for rubber. The strength of this material in uniaxial tension is about 25 MPa in terms of engineering (first Piola Kirchhoff) stress, see Fig. 5, which translates to 125 MPa in terms of true (Cauchy) stress. As can be seen from Fig. 9, there is a region in the vicinity of the crack tip where this stress is exceeded.

The outcome from the analyses is also illustrated graphically in Fig. 10. Results are shown in terms of the energy release rates $J$ and $J_{ff}$, where $J$ represents the energy release rate in the vicinity of the crack tip, whereas $J_{ff}$ represents the work of fracture that needs to be applied externally in order to propagate the crack at steady-state.

From Fig. 10 it appears that the energy release rates increase in an almost exponential fashion with crack speed. It is also clear that below a crack speed of about $v_c = 50$ m/s, the influence of inertia is negligible, i.e. $J_{ff}$ is virtually identical to $J$. Above this speed, however, inertia comes into play and to some extent "shields" the crack

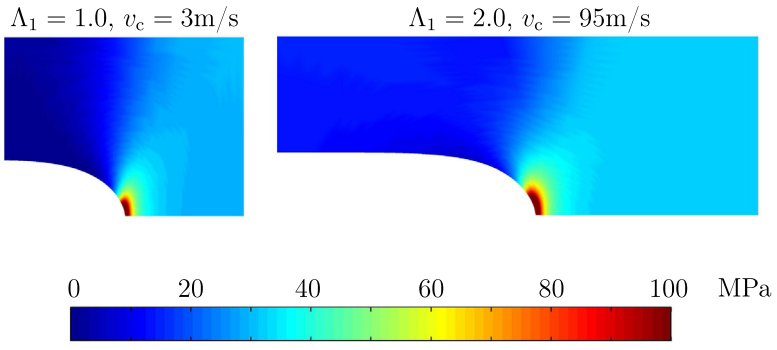



**Fig. 9.** Distribution of maximum principal (Cauchy) stress $\sigma_1$ for two different load cases: $\{\Lambda_1 = 1.0,\ \Lambda_2 = 3.0,\ v_c = 3$ m/s$\}$ and $\{\Lambda_1 = 2.0,\ \Lambda_2 = 3.0,\ v_c = 95$ m/s$\}$.

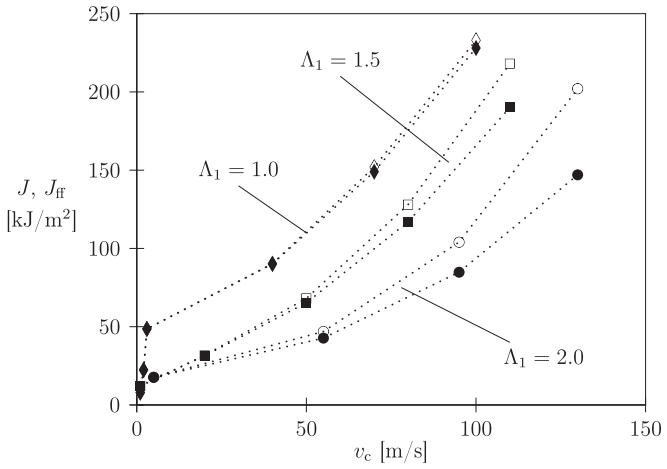



**Fig. 10.** Energy release rates in terms of crack tip $J$ (filled symbols) and far field $J_{\mathrm{ff}}$ (open symbols) at different crack speeds.

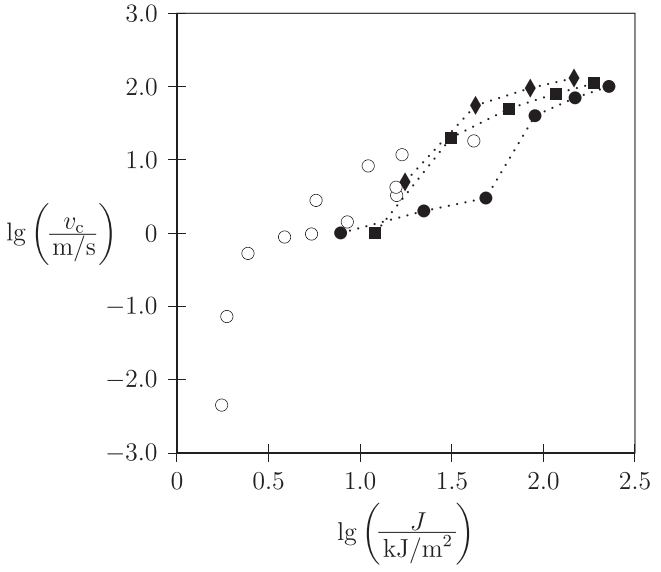



**Fig. 11.** Energy release rates from Lake et al. (2000) ('∘') compared with the computed values of $J$ from the present study (filled symbols according to Fig. 10).

tip from the externally applied work of fracture, i.e. $J < J_{\mathrm{ff}}$. It also seems that for a given crack speed, $v_{\mathrm{c}}$, the effects of inertia increase with the applied transverse stretch, $\Lambda_1$.

## 5. Discussion and concluding remarks

Dissipative processes are of great significance when it comes to the fracture resistance of materials. The purpose of the present study is to shed some more light on these dissipative processes in rubber. A few attempts have been done previously to numerically predict the contribution of viscoelasticity to the resistance to fracture (Carbone and Persson, 2005; Persson and Brener, 2005; Tang et al., 2008, 2009). However, these studies adopt a theory valid for infinitesimal strains, and the validity of those results for rubber-like solids is therefore questionable. In a previous study by the present author (Kroon, 2011), a first attempt was made to predict the contribution of viscoelastic dissipation to the total work of fracture. In that case, the rubber was modelled as a Kelvin material and a state of plane deformation was considered. Further insights were gained in Elmukashfi and Kroon (2012, in press), where full transient dynamic analyses of crack propagation in rubber were performed. The present analysis is an attempt to achieve more insights, and we now consider a biaxially stretched Maxwell material in a state of plane stress.

It should be noted that theoretical predictions as well as experimental observations indicate that the actual separation process at the very crack tip requires an energy release rate of about 50 J/m$^2$ (Lake and Lindley, 1964; Lake and Lindley, 1965; Lake and Thomas, 1967; Mueller and Knauss, 1971; Ahagon and Gent, 1975), which is significantly less than the energy release rates obtained in the present study or in the forgoing studies (Kroon, 2011; Elmukashfi and Kroon, 2012; Elmukashfi and Kroon, in press). However, such estimates are valid for a crack propagating very slowly and at high temperature, for which case viscoelastic dissipation is minimised. Hence, the great difference between such estimates and the present results must be attributed to additional dissipative processes taking place in front of the crack tip. Experimental studies also show that the energy release rate increases with crack speed, and at a crack speed of $v_{\mathrm{c}} = 10$ m/s, for example, the energy release rate is expected to be somewhere in the range 10–100 kJ/m$^2$ (Lake et al., 2000), which is in agreement with the present results, see Fig. 11.

In Fig. 10, it may be observed that for a given crack speed $v_{\mathrm{c}}$, the energy release rates decrease with increasing transverse stretch $\Lambda_1$. This is in line with other experimental observations for quasi-static crack growth (Gent and Kim, 1978). The reason for this is not well understood. However, it may be conjectured that the amount of energy dissipated in the damage process zone is related to the normal stress required to propagate the crack. Hence, the addition of a transverse stress may decrease the normal stress required for crack propagation, which in turn decreases the amount of energy dissipated in the damage process zone.

It is to be expected, that there exists a damage process zone in the vicinity of the propagating crack tip. As a start, we may think of this as a cohesive zone. The estimate of the actual surface energy is 50 J/m$^2$, and we may assume a rectangular cohesive law. The surface energy may then be computed as the strength of the surface times some critical distance between the two crack faces. If we apply the engineering strength of the present rubber, i.e. 25 MPa, the resulting critical surface separation in such a cohesive zone would be 2 μm. Hence, at high temperatures and low crack speeds, the process zone in which dissipation occurs is expected to have a size in the micron range. But if we instead use a typical energy release rate from the present study, say 100 kJ/m$^2$, we instead end up with a characteristic size of 4 mm for the damage/dissipation zone. This estimate seems to agree fairly well with the stress contours in Fig. 9 where the characteristic size of the region in which the stress has exceeded the fracture stress is of the order of a few millimetres.

It is a well-established fact, that in rubber, mode I cracks may attain speeds that exceed the Rayleigh wave speed. This type of super-sonic crack propagation has been examined in previous studies, e.g. by Marder (2006), Zhang et al. (2009) and Chen et al. (2011). For instance, Chen et al. (2011) perform both experimental and numerical examinations of the transition from sub- to super-sonic crack propagation, and the influence of test sample size is investigated. Two different scaling regimes for crack speeds were identified. That is, for subsonic cracks, the crack speeds were independent of the sample size when plotted vs. the stored elastic energy, whereas for supersonic cracks, the crack speed becomes independent of sample size when plotted vs. the applied normal stretch ($\Lambda_2$ in the present study). This outcome seems to be in good agreement with the predictions by Marder (2006), who proposed a theoretical framework for shock-like crack propagation in rubber-like materials. This wedge-like crack tip associated with shock-like

crack propagation was not observed in the present study, even at the highest crack speeds. Instead, the crack profile assumed the typical parabolic shape, usually observed for slowly propagating and static cracks.

In summary, a computational framework for studying high-speed crack growth in biaxially stretched rubber-like solids under conditions of plane stress and steady-state has been proposed. The main purpose has been to investigate the energy release rates required for crack propagation under different modes of biaxial stretching. It was demonstrated, that inertia is expected to come into play when the crack speed exceeds 50 m/s. The total work of fracture by far exceeds the surface energy consumed at the very crack tip, and the difference must be attributed to dissipative damage processes in the vicinity of the crack tip. The size of this damage zone is expected to be a few millimetres.

## References


Ahagon, A., Gent, A.N., 1975. Threshold fracture energies for elastomers. J. Polym. Sci.: Polym. Phys. Ed. 13, 1903–1911.

Bascom, W.D., 1977. Scanning electron microscopy of rubber tear. Rubber Chem. Technol. 50, 875–883.

Bergström, J.S., Boyce, M.C., 1998. Constitutive modeling of the large strain time-dependent behavior of elastomers. J. Mech. Phys. Solids 46, 931–954.

Bhowmick, A.K., Nando, G.B., Basu, S., De, S.K., 1980. Scanning electron microscopy studies of fractured natural rubber surfaces. Rubber Chem. Technol. 53, 327–334.

Carbone, G., Persson, B.N.J., 2005. Crack motion in viscoelastic solids: the role of the flash temperature. Eur. Phys. J. E 17, 261–281.

Chang, S.-J., 1972. Path-independent integral for rupture of perfectly elastic materials. J. Appl. Math. Phys. 23, 149–152.

Chang, J.H., Chen, C.B., 1997. FE calculation of elastodynamic energy release rate for rubbery materials. Finite Elem. Anal. Des. 28, 151–163.

Chen, C.H., Zhang, H.P., Niemczura, J., Ravi-Chandar, K., Marder, M., 2011. Scaling of crack propagation in rubber sheets. Europhys. Lett. 96, 36009/1–36009/6.

Chung, B., Funt, J.M., Ouyang, G.B., 1991. Effects of carbon black on elastomer ultimate properties – IR compounds. Rubber World 5, 46–51.

Deegan, R.D., Petersan, P.J., Marder, M., Swinney, H.L., 2002. Oscillating fracture paths in rubber. Phys. Rev. Lett. 88, 1–4.

de Gennes, P.G., 1996. Soft adhesives. Langmuir 12, 4497–4500.

Dragoni, E., Medri, G., 1988. Fracture toughness evaluation of natural rubber. Theor. Appl. Fract. Mech. 10, 79–83.

Elmukashfi, E., Kroon, M., 2012. Numerical analysis of dynamic crack propagation in rubber. Int. J. Fract. 177, 163–178.

Elmukashfi, E., Kroon, M., in press. Numerical analysis of dynamic crack propagation in biaxially strained rubber sheets. Eng. Fract. Mech. 124–125, 1–17.

Fukahori, Y., Andrews, E.H., 1978. Fracture surface roughness in highly deformable polymers. J. Mater. Sci. 13, 777–785.

Gent, A.N., Kim, H.J., 1978. Tear strength of stretched rubber. Rubber Chem. Technol. 51, 35–44.

Gent, A.N., Marteny, P., 1982a. Crack velocities in natural rubber. J. Mater. Sci. 17, 2955–2960.

Gent, A.N., Marteny, P., 1982b. The effect of strain upon the velocity of sound and the velocity of free retraction for natural rubber. J. Appl. Phys. 53, 6069–6074.

Gent, A.N., Pulford, C.T.R., 1984. Micromechanics of fracture in elastomers. J. Mater. Sci. 19, 3612–3619.

Goldberg, A., Lesuer, D.R., Patt, J., 1988. Observations made during stretching, tearing, and failure of NR and SBR loaded with various amounts of carbon black. Rubber Chem. Technol. 62, 288–304.

Greensmith, H.W., 1956. Rupture of rubber. IV: Tear properties of vulcanizates containing carbon black. J. Polym. Sci. 21, 175–187.

Greensmith, H.W., Thomas, A.G., 1955. Rupture of rubber. III: Determination of tear properties. J. Polym. Sci. 18, 189–200.

Kawabata, S., Kawai, H., 1977. Strain energy density functions of rubber vulcanizates from biaxial extension. Adv. Polym. Sci. 24, 89–124.

Knauss, W.G., 1969. Stable and unstable crack growth in viscoelastic media. Trans. Soc. Rheol. 13, 291–313.

Kolsky, H., 1969. Production of tensile shock waves in stretched natural rubber. Nature 224, 1301.

Kroon, M., 2011. Steady-state crack growth in rubber-like solids. Int. J. Fract. 169, 49–60.

Lake, G.J., Lindley, P.B., 1964. Ozone cracking, flex cracking and fatigue of rubber. Rubber J. 146, 24–30.

Lake, G.J., Lindley, P.B., 1965. The mechanical fatigue limit for rubber. J. Appl. Polym. Sci. 9, 1233–1251.

Lake, G.J., Thomas, A.G., 1967. The strength of highly elastic materials. Proc. R. Soc. London A 300, 108–119.

Lake, G.J., Lawrence, C.C., Thomas, A.G., 2000. High-speed fracture of elastomers: Part I. Rubber Chem. Technol. 73, 801–817.

Li, F.Z., Shih, C.F., Needleman, A., 1985. A comparison of methods for calculating energy release rates. Eng. Fract. Mech. 21, 405–421.

Lindley, P.B., 1973. Relation between hysteresis and the dynamic crack growth resistance of natural rubber. Int. J. Fract. 9, 449–462.

Marder, M., 2005. Shock-wave theory for rupture of rubber. Phys. Rev. Lett. 94, 1–4.

Marder, M., 2006. Supersonic rupture of rubber. J. Mech. Phys. Solids 54, 491–532.

Mueller, H.K., Knauss, W.G., 1971. The fracture energy and some mechanical properties of a polyurethane elastomer. Trans. Soc. Rheol. 15, 217–233.

Niemczura, J., Ravi-Chandar, K., 2011. On the response of rubbers at high strain rates. III: Effect of hysteresis. J. Mech. Phys. Solids 59, 457–472.

Pandey, K.N., Mathur, D.K.S.G.N., 2003. Fracture topography of rubber surfaces: an SEM study. Polym. Test. 22, 353–359.

Persson, P.N.J., Brener, E.A., 2005. Crack propagation in viscoelastic solids. Phys. Rev. E Stat. Nonlinear Soft Mat. Phys. 71, 1–8.

Persson, P.N.J., Albohr, O., Heinrich, G., Ueba, H., 2005. Crack propagation in rubber-like materials. J. Phys.: Condens. Mat. 17, R1071–R1142.

Petersan, P.J., Deegan, R.D., Marder, M., Swinney, H.L., 2004. Cracks in rubber under tension exceed the shear wave speed. Phys. Rev. Lett. 93, 1–4.

Rahulkumar, P., Jagota, A., Bennison, S.J., Saigal, S., 2000. Cohesive element modeling of viscoelastic fracture: application to peel testing of polymers. Int. J. Solids Struct. 37, 1873–1897.

Rajaram, H., Socrate, S., Parks, D.M., 2000. Application of domain integral methods using tetrahedral elements to the determination of stress intensity factors. Eng. Fract. Mech. 66, 455–482.

Rice, J.R., 1968. A path independent integral and the approximate analysis of strain concentration by notches and cracks. J. Appl. Mech. 35, 379–386.

Rivlin, R.S., Thomas, A.G., 1953. Rupture of rubber. I: Characteristic energy for tearing. J. Polym. Sci. 10, 291–318.

Schapery, R.A., 1975. A theory of crack initiation and growth in viscoelastic media. Int. J. Fract. 11, 141–159.

Schapery, R.A., 1989. On the mechanics of crack closing and bonding in linear viscoelastic media. Int. J. Fract. 39, 163–189.

Setua, D.K., De, S.K., 1983. Scanning electron microscopy studies on mechanism of tear fracture of styrene–butadiene rubber. J. Mater. Sci. 18, 847–853.

Shih, C.F., Moran, B., Nakamura, T., 1986. Energy release rate along a three-dimensional crack front in a thermally stressed body. Int. J. Fract. 30, 79–102.

Tang, S., Guo, T.F., Cheng, L., 2008. Rate effects on toughness in elastic nonlinear viscous solids. J. Mech. Phys. Solids 56, 974–992.

Tang, S., Guo, T.F., Cheng, L., 2009. Dynamic toughness in elastic nonlinear viscous solids. J. Mech. Phys. Solids 57, 384–400.

Thomas, A.G., 1955. Rupture of rubber. II: The strain concentration at an incision. J. Polym. Sci. 18, 177–188.

Thomas, A.G., 1994. The development of fracture mechanics for elastomers. Rubber Chem. Technol. 67, G50–G60.

Wang, W., Chen, S., 2005. Hyperelasticity, viscoelasticity, and nonlocal elasticity govern dynamic fracture in rubber. Phys. Rev. Lett. 95, 1–4.

Zhang, H.P., Niemczura, J., Dennis, G., Ravi-Chandar, K., Marder, M., 2009. Roughening effects of strain-induced crystallites in natural rubber. Phys. Rev. Lett. 102, 245503/1–245503/4.